AIAA-94-2740

Segmented Ion Engine Plume Characteristics

C. Michael Tierney*, John R. Brophy, Juergen Mueller*****
Jet Propulsion Laboratory
California Institute of Technology
Pasadena, California

Preliminary evaluation of the segmented ion thruster (SIT) ion beam characteristics was performed by measuring the two dimensional ion current density distribution at four axial locations downstream from the thruster. Current density profiles were measured with the concurrent operation of multiple ion sources. Preliminary assessments regarding symmetry of the plume, characterization of plume development as a function of axial position, and the interactions of multiple simultaneously operating ion sources were conducted. A numerical integration scheme was applied to the acquired data to determine the total beam current. These calculated values were generally within 5% of the values measured by the SIT power processing electronics. Asymmetries of the ion beam about the centerline of the ion source were observed for segments A and C. A qualitative analysis of the downstream development of the ion beam was conducted. The widening of the beam and increase in uniformity of the current density were noticed. The reconstruction of current density profiles produced from simultaneous operation of multiple ion sources using data obtained from the operation of single ion sources was attempted. Unfortunately this produced only limited success. An initial assessment of the divergence of the plume found that a 10° half cone angle would contain most of the ion beam. Most of the data acquired thus far has been on somewhat of a trial basis and extensive testing is scheduled to resume in August 1994.

Nomenclature

x= Position of Traverse with Respect to Origin Along X Axis
Y= Position of Traverse with Respect to Origin Along Y Axis
Z= Position of Traverse with Respect to Origin Along Z Axis

Introduction

The segmented ion thruster is being developed by JPL for potential application to solar system exploration missions, [l] As shown in Figs, 1 and 2, the segmented ion thruster consists of four separate ion sources, each with its own 3 grid ion optics. Each of these ion sources can be operated independently or in any combination, This capability facilitates throttling of the segmented ion thruster to accommodate the reduction of available power from solar arrays as the spacecraft's orbit trajectory moves farther from the Sun.

As with any ion thruster used for spacecraft propulsion, important operating information, including thruster lifetime, spacecraft contamination, and ion optics performance, can be derived from characteristics of the exhausted ion beam. Operation of the segmented ion thruster raises additional issues which can be resolved

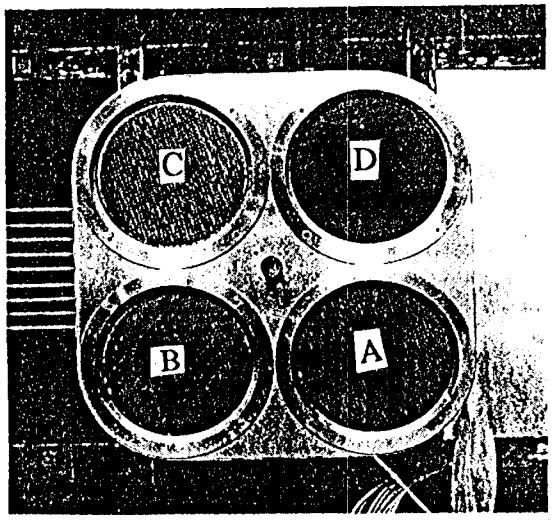

Figure 1

---

* Graduate Student, Department of Aeronautics, California Institute of Technology
** Supervisor, Advanced Propulsion Technology Group, JPL
*** Member of the Technical Staff, Advanced Propulsion Technology Group, JPL

through analysis and characterization of the exhausted ion beam. This includes multiple ion beam interaction and the resulting impact on the lifetime, contamination, and optics performance. Likewise, repeatability of construction and operation of the individual ion sources can be addressed.

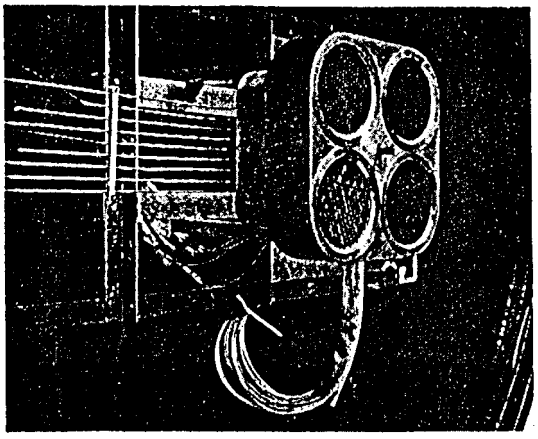

Figure 2

Thus far in performance of the segmented ion thrust plume characterization the ion current density profile of individual and a single pair of ion sources have been investigated, In relation to the lifetime issues, the ion current density profile will assist in the understanding of grid erosion mechanisms due to regions of high or low ion impingement rates, The divergence of the *ion* beam will aid in evaluation of spacecraft integration issues. Performance of the ion grid optics can be assessed through evaluation of the current density profile which include evaluation of grid hole alignment,

Apparatus

Test Facilities

Testing was conducted in a 2.4 m-dia. x 5 m long stainless steel vacuum facility with an effective pumping speed on Xc of -14,000 L/s, A more detailed description of the facility and segmented ion thruster support hardware is given if Ref. 1.

Segmented Ion Thruster

The 4x15-cm segmented ion thruster shown in Fig, 1 is made up of four 15-cm diameter ion sources of the type described in Ref. 2. Each ion source is a modified, scaled-down version of the NASA light-weight, 30-cm diameter ring-cusp thruster[3]. Each discharge chamber body is made of 6061 aluminum and the ring-cusp magnetic field configuration is formed from two rings of samarium-cobalt magnets; onc positioned at the upstream end near the cathode and the other at the downstream end near the accelerator systcm. Two of the ion sources have the polarity of their magnet rings reversed to give a right- and Ieft-handedness to the sources. In the segmented engine configuration, the ion sources (or segments) are integrated such that segments A and C are right-handed and B and D arc left-handed.

The ion source segments are integrated onto a base plate structure at ground potential. Electrical insulators between the segments and to the centrally located neutralizer assembly are used to make the overall structure very rigid. Each ion source is electrically isolated from the others. Electrical integration of the ion source segments is accomplished at the power supplies. This enables a faulty ion source to be isolated from the others. A single, centrally-located neutralizer cathode is used to neutralize all of the ion sources. For a propulsion system which consists of a single segmented ion engine, a second neutralizer cathode would likely be included for redundancy.

Operational Characteristics

The following table lists the relevant operating characteristics of the segmented ion thruster for the tests described in this paper.

Table A

Parameter	Value
Beam Current	425 mA
Screen Voltage	1303 V
Accelerator Grid Current	2.51 mA
Accelerator Grid Voltage	-151 V
Decelerator Grid Current	4.05 mA
Decelerator Grid Voltage	-105 V
Discharge Current	3.0A
Discharge Voltage	27.9 V
Keeper Current	0.45 A
Keeper Voltage	6.8 V
Main Flow Rate	5.49 sccm
Total Discharge Chamber Flow Rate	6.84 sccm
Neutralizer Keeper Current	4.01 A
Neutralizer Keeper Voltage	18.8 V
Coupling Voltage	3.8 V

Grids

Three-sets of 3-grid ion accelerator systems were fabricated from carbon-carbon. A fourth set was damaged during fabrication and couldn't be used. Ion source segments A, B, and C were equipped with the carbon-carbon grids. Segment D was equipped with a 3-grid, graphite accelerator system as described in Ref. 2. The geometries of the carbon-carbon and graphite grids are

summarized in Ref. 4 as arc details of the fabrication and operation of the carbon-carbon grids,

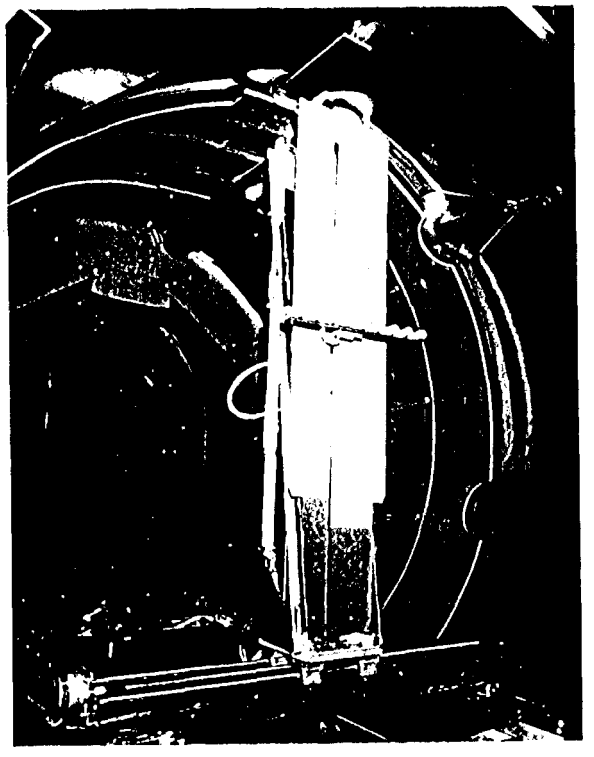

Figure 3

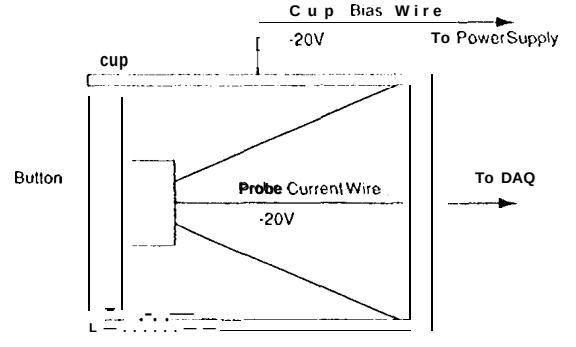

Figure 4

Probe System

The probe system as shown in Fig. 3 consists of nine Faraday cups mounted to a 3-axis, computer controlled probe positioning system. These cups are horizontally mounted with 5 cm center spacing between each probe. As shown in Fig, 4, the probes arc composed of two primary pieces, the button and the cup, 'f'he button and cup are electrically isolated.

The face of the button (side which is pointed towards the ion source), is 2.3 cm in diameter and is coated with ~0.1 cm of tungsten. This coating is used in order to reduce the secondary electron emission associated with the impinging ion beam. In order to repel free electrons in the ion beam the button and cup arc biased -20 V with respect to the surrounding kink wall. The neutralizer common (o ground potential was typically -5 V during operation,

Probe Positioning System

The probe rake is mounted on a 3-D traverse mechanism as shown in Fig. 3. This traverse mechanism uses pillow blocks supported by slide rails with ball screws and stepper motors for motion control,

The coordinate axes of the traverse mechanism are as follows: X axis - Left/Right, Y axis - Up/Down, Z axis Front/Back. The origin of these axes correspond to X,Y,Z = 0,0,0 and is located in the upper left hand corner of the tank with the traverse as C1OSC to the thruster as limit switches will allow. Positive X travel is from left to right (facing in the direction of beam propagation), positive Y travel is from top to bottom, and positive Z travel is from front to rear. The position Z=O corresponds to a position approximately 5 cm from the face of the engine.

The motion of the traverse mechanism was controlled by a Macintosh Centris 650 computer with LabView software, a digital 1/0 board and stepper motor driver electronics. In order to know the position of the traverse mechanism, the LabView software counted the number of TTL pulses transmitted to the stepper motor drive electronics and knowing the lead of the ball screw, the computer calculates the location of the traverse with respect to the starting position,

Data Acquisition System

The Faraday cups were each connected across precision resistors. A voltage conversion module converts the voltage drop read across the resistor (-50 mV to +50 mV) to a -5V to +5V signal which could be read by an analog 1/0 board resident within the Macintosh computer. As mentioned above, the LabView data acquisition software was used in order to control both the motion of the traverse mechanism, and the acquisition and archiving of the raw probe data,

The LabView software was configured so that at each probe position seven data elements were saved in a row configuration with standard ASCII text format. These data elements consisted of the probe number, the average value of 200 probe samples, the standard deviation of these 200

samples, the X, Y and Z coordinates for each probe (as opposed to the X,Y,Z coordinates for the traverse), and the time at which the data was taken. Each of these data elements correspond to a column with in the archived file,

Procedure

Test Performance

With the vacuum chamber at a static pressure of 1.33 x 10-3 Pa, the segmented ion thruster operating at the parameters specified above in Table A, the probe positioning system placed the Faraday cup rake at an initial X,Y,Z position and then proceeded to move the probe rake in a zig-zag fashion from left to right and top to bottom, The traverse mechanism would stop at predetermined X, Y positions and data was acquired from each probe. The probes were positioned with either 2.5 cm or 5 cm spacing in the X and Y directions. (2,5 cm spacing for Z locations of 30.5 and 61,0 cm and 5 cm spacing for Z locations of 91.5 and 122.0 cm). The traverse mechanism used to obtain X-Y beam current density maps at four different positions downstream from the thruster. Duc to the geometry of the probe rake and operation of the traverse mechanism, instances existed where data was acquired from the same location more than once. This simply added data to the system and caused a minimal inconvenience in the data reduction and analysis.

The LabView program was configured so that the operator could specify the total area of probe coverage, the initial starting position for data acquisition, and the spacing between measurements. This allowed the operator to make a rough estimate as to the total area to be scanned, thus reducing the time necessary to acquire an X-Y plane of data.

Thruster Operation

Each of the ion sources equipped with carbon-carbon girds (segments A,B&C) were operated individually and beam current density maps obtained at Z positions of 30.5,61.0, 91,5 and 122,0 cm. The plan was then to operate the ion sources in pairs and finally all four at once, Grid problems with segment D would not permit sufficiently stable operation to obtain beam profile scans, therefore, data was taken for only segments A, B, and C. Duc to technical problems with the probe positioning system and scheduling constraints the only multiple ion source operation for which data could bc obtained was for segments B&C.

Data Reduction and Transformation

The data acquired by the computer consisted of X, Y, Z locations of the particular probe, and a measurement of the current generated by the ion impingement on that probe. The units of X, Y, Z locations arc in inches because the dimensions of the ball screws from the manufacturer arc in English units. These measurements were converted to metric units for processing to be done later. In addition, the raw probe current readings (mA) were transformed to current densities (mA/cm^2). There was however, the need to determine the appropriate viewing area of the probes to the thruster in order to transform the current to current density. As the probes move off the centerline of the ion source the area normal to the thruster decreases from the nominal $4.104 cm^2$. This is simply a trigonometric transformation of the area, The geometry to determine the angle for transformation is shown in Fig, 5. This viewing area was not taken into account for the multiple segment operation due to the uncertainty in determining the appropriate angle for transformation.

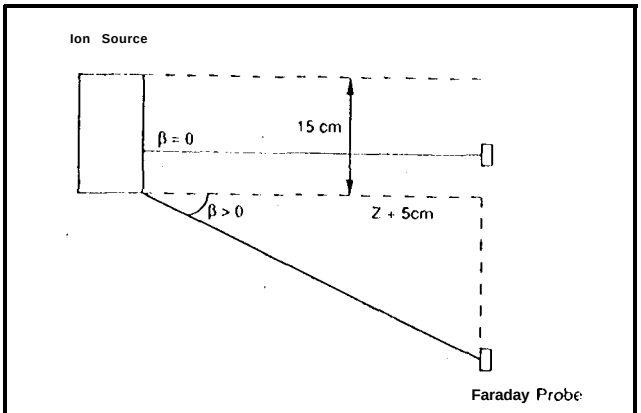

Figure 5

As discussed above, there were instances of multiple current samplings for the same probe locations, This results, however, in an unacceptable format for some of the post data processing techniques that were used, In order to alleviate this problem, the multiple current readings were simply averaged and this average value was used for all subsequent processing,

Data Analysis

The first step in the analysis of the data obtained was to calculate the total beam current extracted from the thruster. The procedure outlined below was used for data obtained from operation of individual ion source as well as the B-C pair. This was accomplished by using Microsoft Excel to sort the data such that the data was ordered first with respect to X and second with respect to Y. Once this was done, a simple application of Simpson's 3/8 Rule for numerical integration could be made to integrate the beam profile. The first of a double integration was done with Y as the variable of integration for each value of X. Next, the same numerical integration schemes were applied to integrate the values previously obtained with X as the variable of integration. After multiplying this resulting value by an area transformation constant the final resulting

value should be the total beam current extracted from the thruster, This area transformation is the ratio of the area of a square with side length 2.29 cm to the area of a circle with a diameter of 2.29 cm. Fig. 6 shows the current profile as measured by the probes. The integration discussed above is simply a double integration over this surface which determines the volume contained within the contour. An advantage of this technique is that is doesn't require the ion beam current density profile to be symmetric,

Both two dimensional and three dimensional contour plots of the current density as a function of X and Y were generated using DeltaGraph Pro. This was done at each Z position for each ion source operating combination. This allowed for qualitative comparisons of beam profiles between each ion source at the four Z positions. In addition, a graphical progression of the extracted ion beam was developed as a function of Z position (for both individual ion source operation and multiple ion source operation).

Slices of data passing through the center of the extracted ion beam along both the X and Y axes were generated. This was done for each individual ion source operation combination at each Z location. When these X and Y slices were plotted along the same set of coordinates and compared a qualitative evaluation as to the symmetry of the exhausted ion beam was made. Additionally, these slices were plotted such that the different Z locations were superimposed upon one another. This allowed for a qualitative evaluation as to the development of the extracted ion beam as a function of distance from the thruster (Z),

A test for repeatability was conducted to evaluate the performance of the thruster and the data acquisition system. Four sets of data were taken for Segments B&C operating, A slice in the Y direction (at a constant value of X and Z = 30.5 cm) through the center of the B-C plume was extracted from each set of data and compared.

A comparison was conducted to look for any evidence of beam interactions when multiple ion sources arc simultaneously operating. Data was obtained for the operation of Segment B and Segment C alone along with operation of Segments B & C together. The data from Segment B operation was added mathematically to the data from Segment C operation and compared to the data obtained from Segments B & C operation. This was not just a simple overlay of the two data set on the same contour plot. Duc to errors in the data obtained from the operation of Segment C at Z = 91.5 cm and Z = 122.0 cm, only the data at Z = 30.5 cm and Z== 61,0 cm was used.

Finally, an attempt to characterize the divergence of the plume was conducted. This involved the placing of a circles upon the 2-D current density contour plots of Segment B at Z = 30.5, 61.0, 91.5, and 122.0 cm. As demonstrated in Fig. 7, these circles correspond to the divergence angles of 5° and 10°. This method does not give an accurate determination of the plume divergence angle, but it will give a qualitative understanding as to how the plume widens with distance from the thruster.

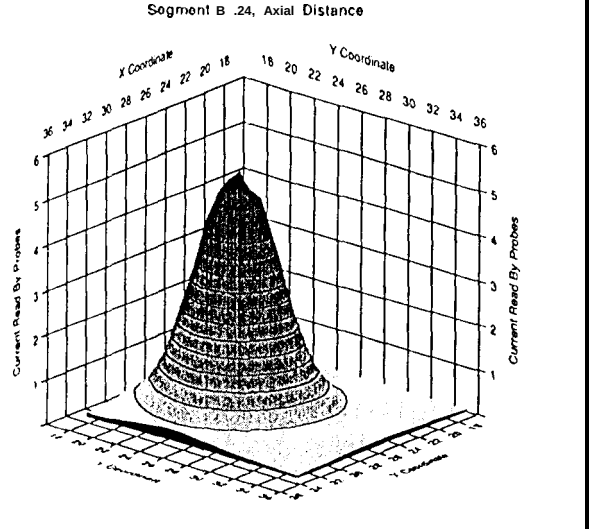

Figure 6

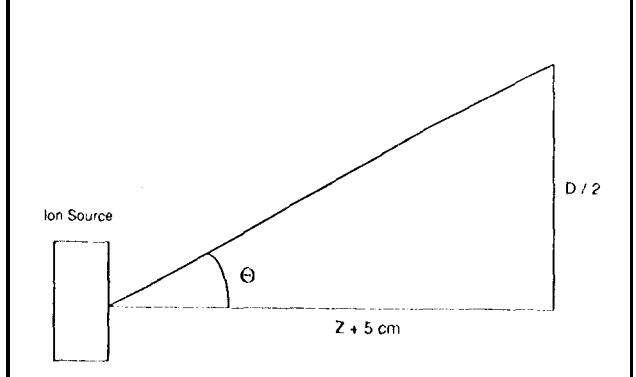

Figure 7

Results and Discussion

Beam Current Integration

A compilation of the integrated beam currents for the different segment operation combinations and distances downstream from the origin is given in Table B. The nominal operating beam currents for all these data were 425 mA per segment. The only exception is for the operation of Segment C at Z = 91.5 cm and at Z = 122.0 cm,

Table B

Segment	Z (cm)	Calculated Beam Current (mA)
A	30.5	418.35
A	61.0	374.40
A	91,5	403.70
A	122.0	360.07
B	30.5	409.22
B	30.5	404.33
B	61.0	405.74
B	91.5	405.90
1?	122,0	371.48
c	30.5	413.80
C	61.0	390.39
C*	91.5	382.98
C*	122.0	334,87
B&C	30,5	748,40
B&C	30.5	811.62
B&C	30.5	805.18
B&C	30.5	813,38
B&C	61.0	770.99
B&C	61.0	733.27
B&C	91.5	669.68
B&C	122.0	635.05

As can be seen from Table B, the calculated total beam current is within ±5% of the expected value for many of the test cases and within ± 15% of the expected value for almost all of the test cases. There arc two primary mechanisms for these di fferences bet ween the expected and calculated values. The first is that the total beam current is decreasing with distance from the thruster. This is primarily duc to charge exchange between the ions. Although this is an important factor, it should be no more than approximately 1% for the vacuum tank back pressures experienced during these tests. The second and more likely mechanism is that the range of motion specified for the probe rake was too small. 'I'his is evident in most of the 3-D current density contour plots shown below. At the edges of the contours, which correspond to the specified limits of the traverse motion, significant portions of the ion beam were not sampled. Although the current density is relatively small in these regions compared to the center of the beam, the area over which the current density should be integrated is substantial. This results in a calculation of the total beam current that could be significantly less than the expected value. Specifying a larger travel area for the probes during data acquisition should rectify this problem.

Also evident in the 3-D current density contour plots shown below, for the case of Z = 30.5 cm, the peak of the contour has been clipped. This clipping was duc to saturation of the voltage conversion modules. Resizing the resistors for a higher maximum peak current density should correct this problem.

Current Density Profiles

Figs, 8-10 depict the current density profiles for segments A, B and C at a Z position of 61,0 cm, Part (a) of each of these figures is the 2-D contour plot corresponding to the 3-D plots in part (b).

The shapes of the 2-D and 3-D current density contours are of importance because of their relation to grid erosion. Regions of higher current density will cause greater erosion than regions of lower current density. Ideally it is desirable for an extracted ion beam to bc uniform in magnitude over the surface of the grids.

It can bc observed in the 3-D contour plots that the beam current is relatively high in the center and falls off rapidly at the edges. Unfortunately the data taken thus far is at least 35 cm from the grid surface. A detailed understanding of the current density profile at the grid surface is not possible with this data, However, it can bc inferred, that based upon the data collected, the current density toward the center of the ion source will be higher than found at the edges of the ion source, Further testing with data taken close to the grid surface is planned.

Onc of the more prominent characteristics of the contour plots found in Figs. 8b, 9b and 10b is the difference in shape between the three ion sources. The 2-D contour plots of segment A and segment C arc largely elliptic.al in shape as opposed to the circular shape expected. The 2-D contour plot of segment B is significantly more circular than segments A and C. However, a slight elongation in the Y direction of the segment B contour plot is visible. These elliptical shapes imply that the plumes are not symmetric about the ion source center line.

It is also of interest to note that the orientation of the elliptical contour plots arc not the same for each segment, The contour plot from segment A is angled such that the semi-major axis of the contour is rotated approximately 10° from the Y axis in the counterclockwise direction. Segment B seems to bc oriented in a similar fashion,

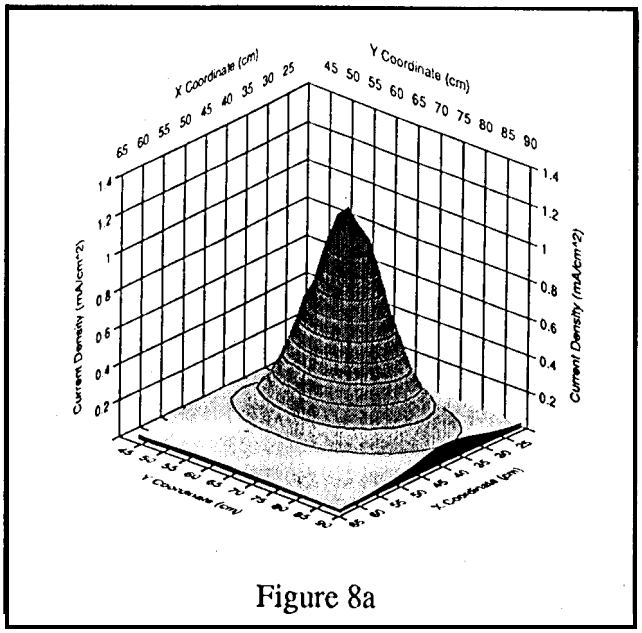

Figure 8a

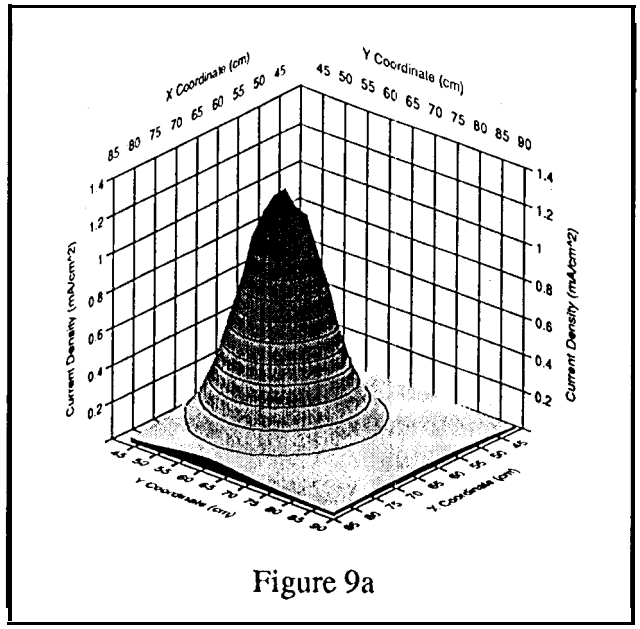

Figure 9a

Segment A Current Density (mA/cm^2)
Z = 61.0 cm

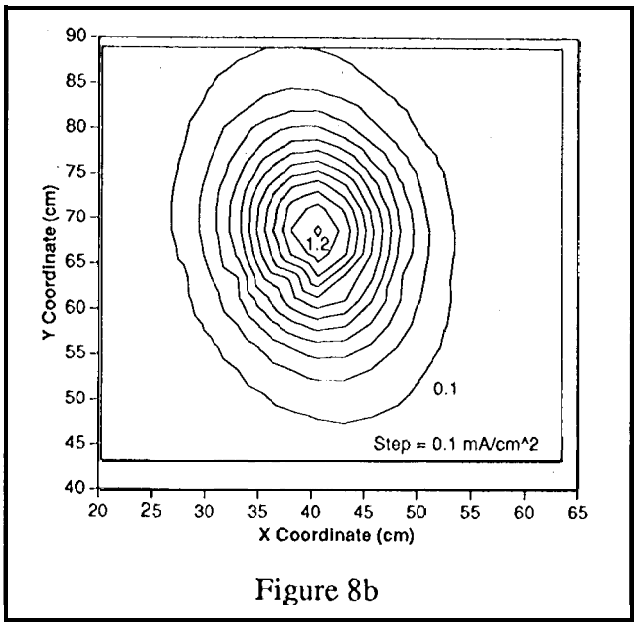

Figure 8b

Segment B Current Density
Z = 61.0 cm

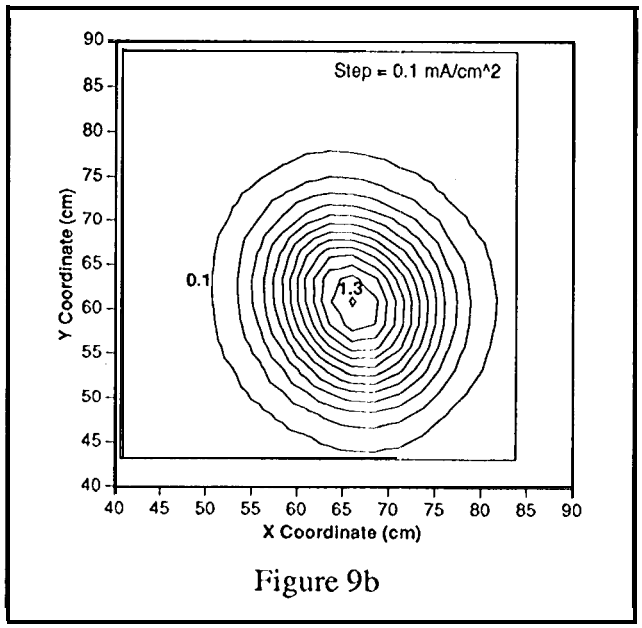

Figure 9b

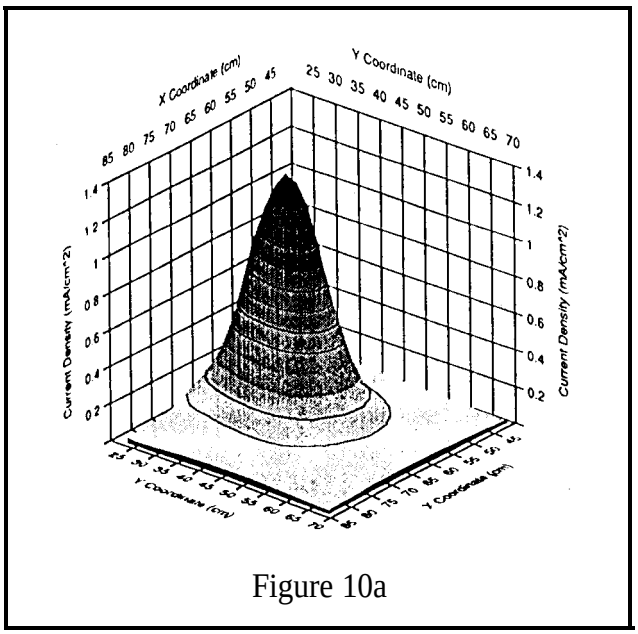

Figure 10a

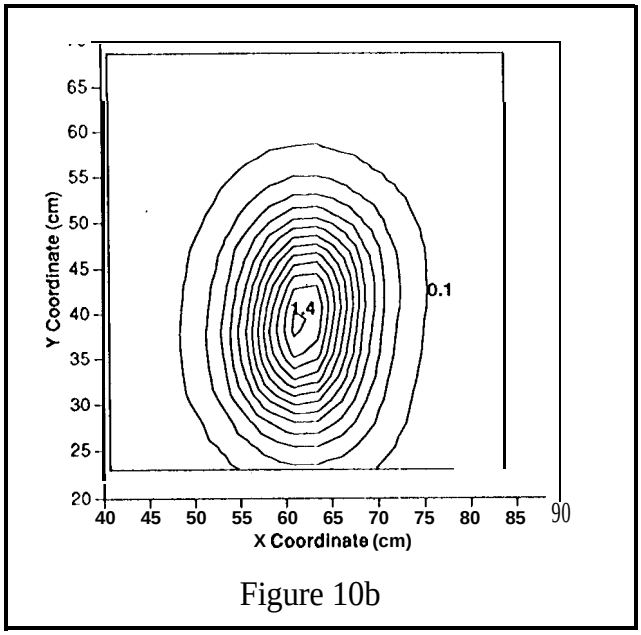

Figure 10b

however, segment C is oriented such that the semi-major axis is almost aligned with the Y axis.

Three potential causes for the elliptical shape of the contours have been identified. The first is some sort of coordination error between the probe positioning system (PPS) the computer. If the PPS does not move exactly as the computer expects then a distortion of the contour plots will result. Although this could sufficiently explain the elongation of the 2-D contour plots, it does not lend itself to an adequate explanation as to the different orientations between the three segments. In addition, an initial assessment as to the repeatability of the PPS was made. The repeatability seemed to bc quite acceptable. According to the 2-D contour plots, the elongation and orientations are different for each segment which would imply a low level of repeatability. Further testing of the traverse mechanism is required in order to evaluate this possibility. A second potential cause is misalignment of the grids. If the holes in the screen, accelerator, and decelerate grids arc not accurately aligned, it is conceivable that the 2-D contour plots would bc skewed in some manner. Evaluation of the alignment of the grids could help assess this possibility. The last possibility identified is some sort of local warping of the grids. The grids used, as stated above, arc made from flat carbon-carbon panels. Thermal warping could cause misalignment of the grid holes as discussed above, again resulting in a distortion of the current density contour.

The existence of elliptical current density contour plots suggest that the ion beams extracted do not have symmetrical geometries about the centerline. Figures 11-13 were generated in order to better evaluate this. The profiles in Figs. 11-13 arc slices of data that run approximately through the centerline of the plume and parallel to the X and Y axes. If the plumes arc symmetric about the centerline and the slices are along this centerline, the X and Y slices should bc identical in shape and size. Unfortunately the operation of the probe positioning system did not allow for slices to cut directly through the centerline of the plume and some uncertainty as to whether the plumes arc symmetric was introduced. However, this uncertainty can not account for the large discrepancies between the X and Y slices in Figs. 11 and 13. The difference between the X and Y slices in Fig. 12, however, could possibly bc explained by this uncertainty.

This evaluation of the current density profile adds to the belief that segments A and C produce asymmetric plumes while segment B produces an almost symmetric plume.

Plume Symmetry Evaluation

Figures 11-13, as shown below, arc plots depicting the current density along X and Y slices through the center of the extracted ion beam. This was done for each ion source operated individually. Comparison between the X and Y slices gives an indication of the plume symmetry. The reasons for the observed asymmetry in segments A&C arc not known,

Current Density Spatial Development

Figures 14-17 arc an initial step in understanding and describing ion beam evolution as a function of downstream position. The shape of the plume begins with a large concentration of ions in the center of the beam and the current density decreases rapidly with radial distance from the centerline. As the ions move further downstream the current density profile becomes wider and with a lower peak. The peak current density at 35 cm downstream from

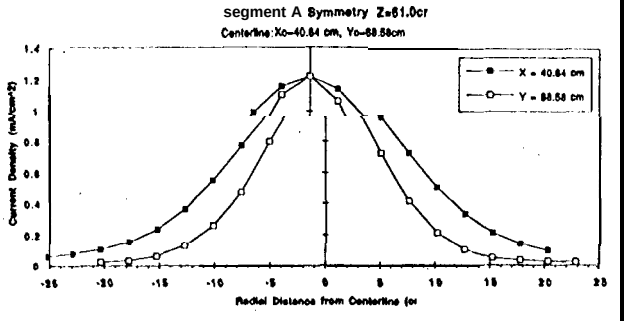

Figure 11

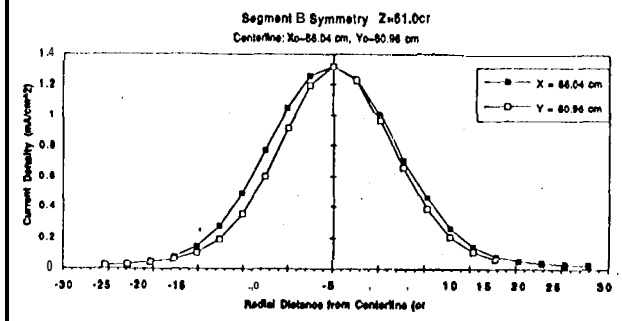

Figure 12

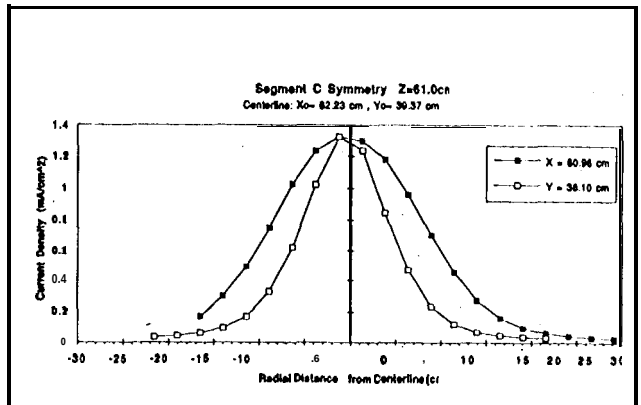

Figure 13

the ion source is about 1.8 mA/cm^2, 127 cm from the ion source the peak current density is about 0.4 mA/cm^2. Although the peak of the current density decreases to about 22% of the current density at Z = 30.5 cm, the total measured beam current decreases only a few percent. Therefore, the base of the current density profile becomes wider as the distance from the ion source increases.

A similar set of 3-D contour plots pertaining to the operation of segments B&C can be found in Figs. 18-21. The peaks at Z = 30,5 cm are similar in size and shape to those found for single ion source operation. As Z increases this similarity begins to diminish. At Z = 122,0 cm the current density profile looks like that from a single operating ion source except for the fact that the total integrated beam current is around 800 mA which corresponds to the operation of two ion sources. Figure 22 also shows this development of the plume as Z increases.

System Operation Repeatability

The slices of data obtained for a constant value of Y through the center of the ion beam extracted from the operation of segments B&C are shown in Figs. 23 and 24. Four separate sets of data were acquired at a Z location of 30.5 cm. Figure 23 shows these data curves without any data adjustment. However, Fig. 24 depicts the same data except that the curves for Series 1 and 2 were shifted by 3 cm to the left. This shift is believed to be the result of probe positioning error and this 3 cm shift was most likely caused by slipping of the Y traverse because of gravity or possibly error in the setting of the traverse at the origin (0,0,0). This problem was noted in other tests and will be corrected in the future.

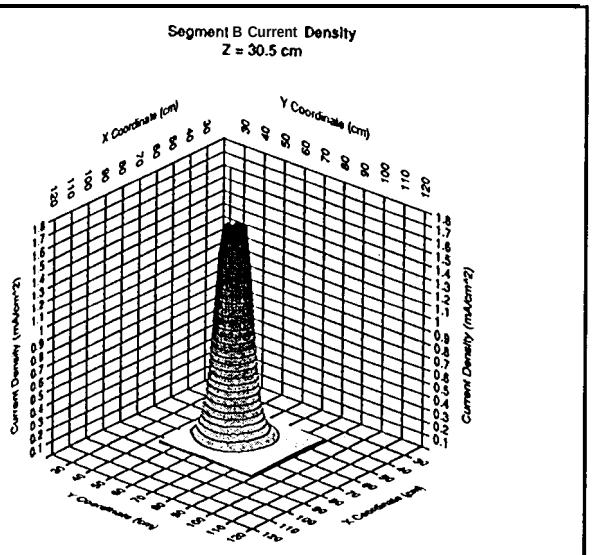

Figure 14

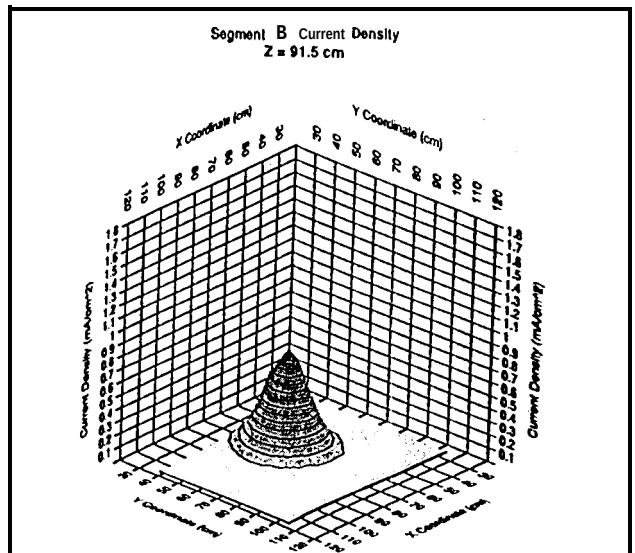

Figure 16

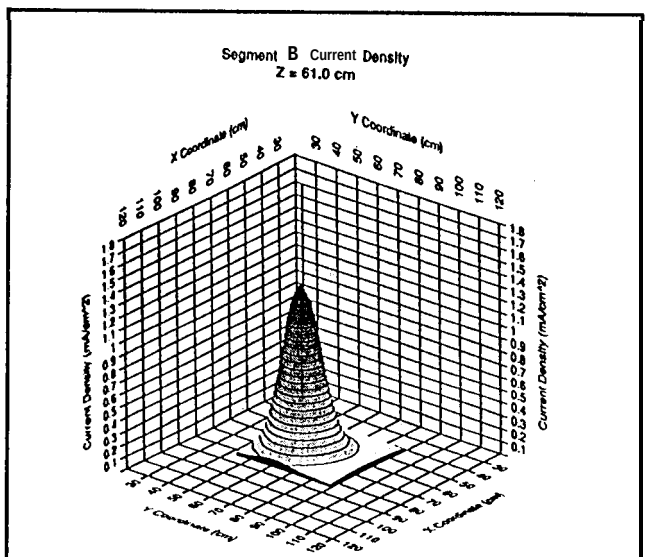

Figure 15

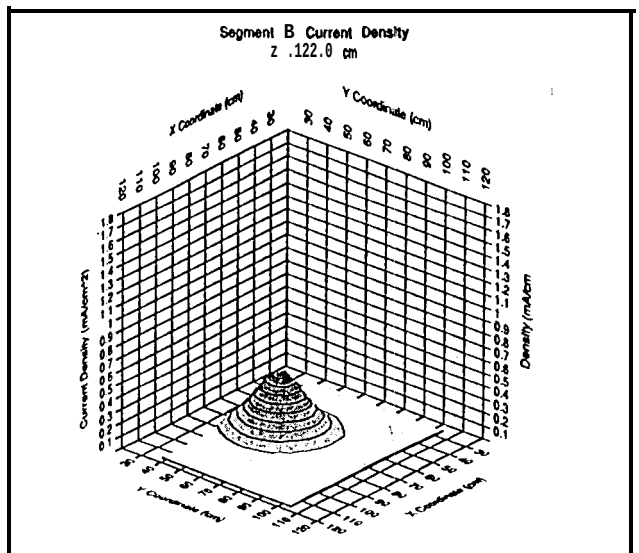

Figure 17

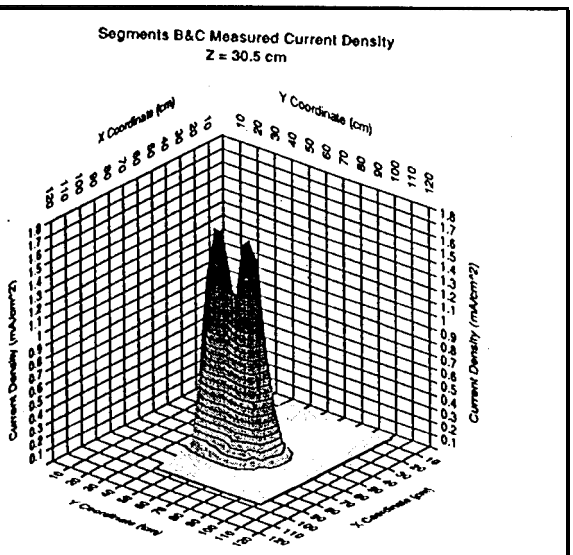

Figure 18

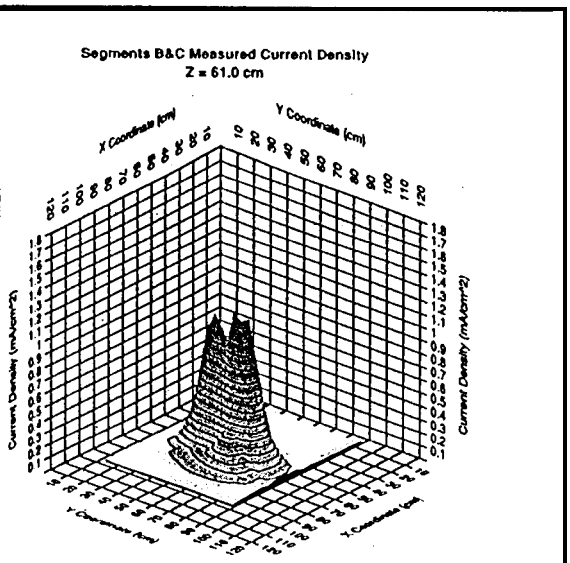

Figure 19

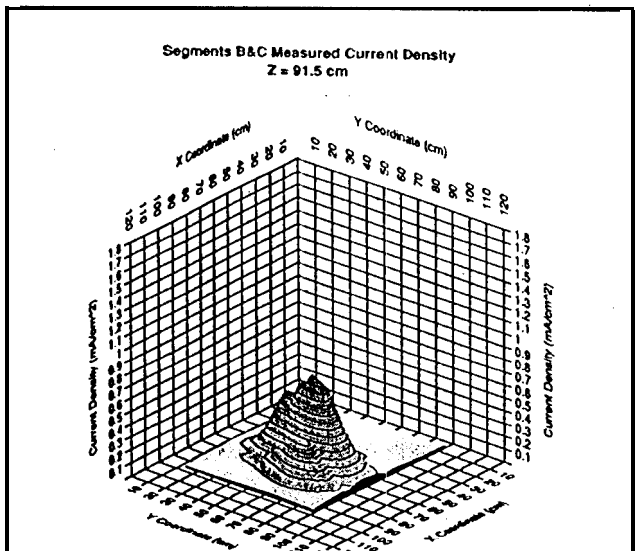

Figure 20

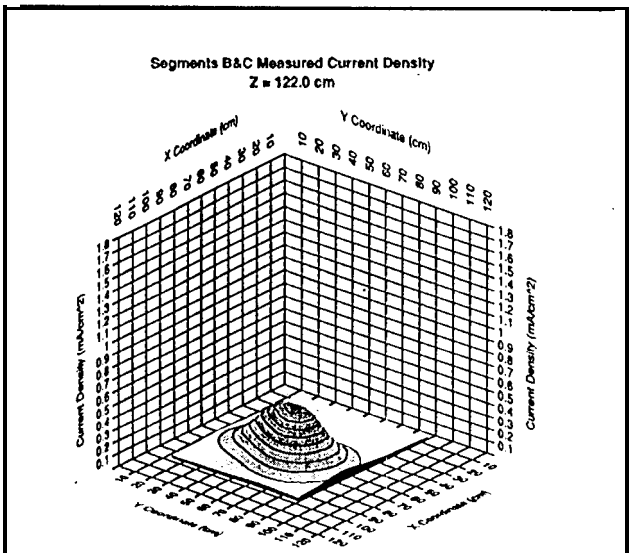

Figure 21

Other than the 3 cm shift of the dam, the profiles all seem to fit well with each other thus demonstrating that the systcm can be operated with a satisfactory level of repeatability.

Multiple Beam Interaction

The current density 3-D contour plots for the simultaneous operation of Segments B & C arc compared to the resulting 3-D contour plots for the mathematical addition of Segment B operation with that of segment C operation. This is shown in Figs. 25 and 26 for Z=30.5 and 61.0 cm, respectively.

The primary differences between the 3-D contour plots using measured data compare to those using mathematically added data is in the region between the ion sources. The peaks of the profiles are about the same and arc in approximately the same locations, but the regions lying between the peaks arc quite different. For Z = 30.5 cm, the measured profiles seem to have current densities of about 1,2 mA/cm^2 between the peaks, and the calculated profiles seem to have current densities of about 0.6 mA/cm^2 between the peaks. This same phenomena occurs at Z = 61.0 cm.

The cause of these differences could possibly be due to limitations of the software used to create the contour plots or it could be a real effect. More data is necessary to better address this,

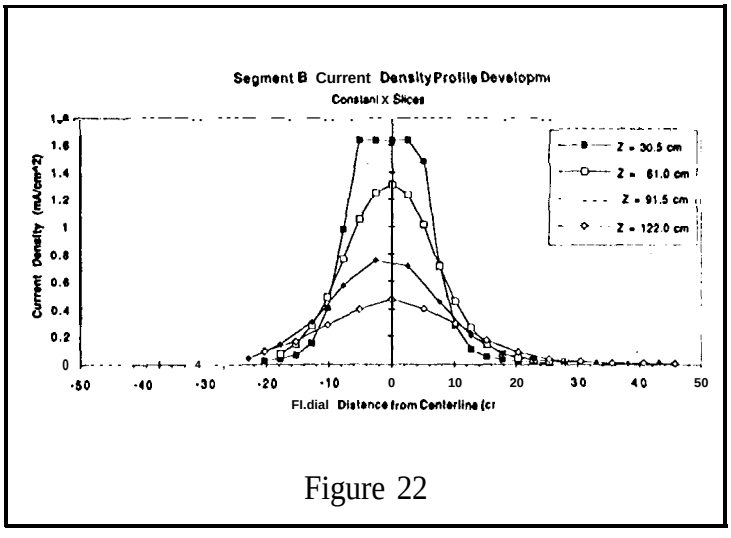

Figure 22

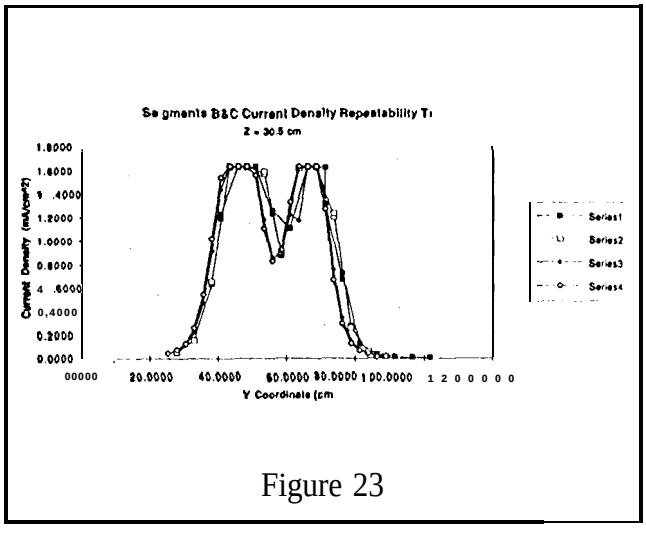

Figure 23

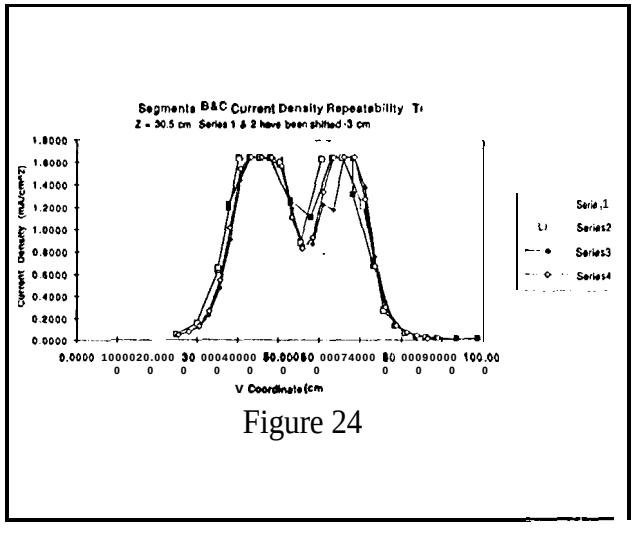

Figure 24

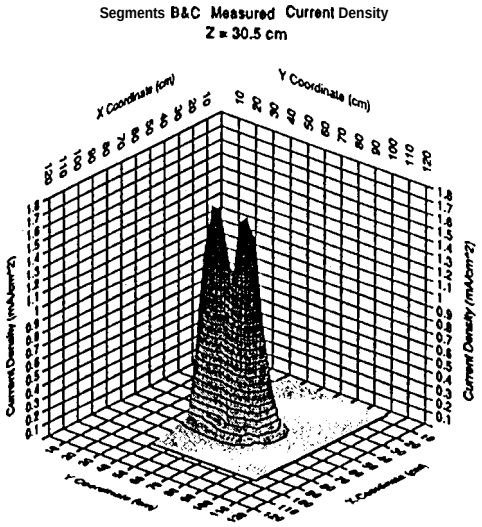

Figure 18

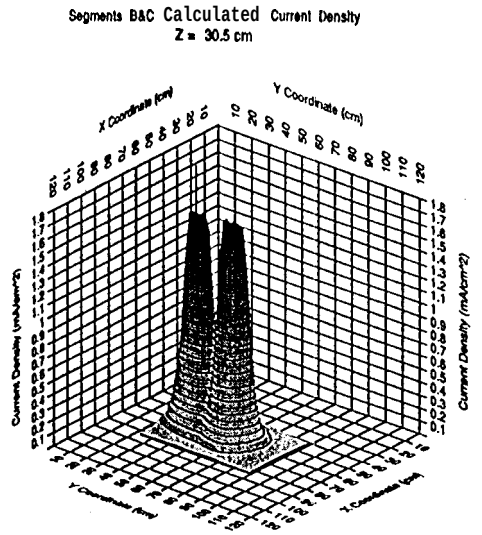

Figure 25

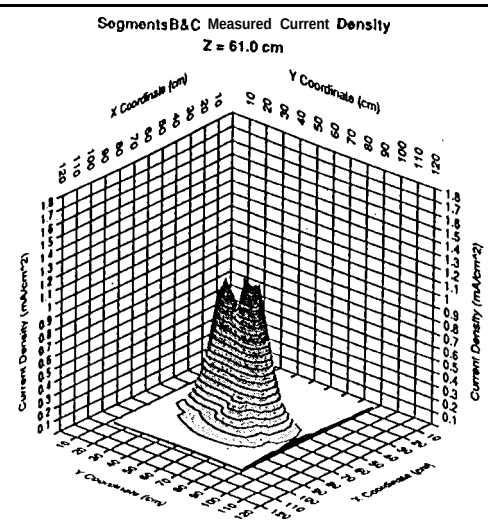

Figure 19

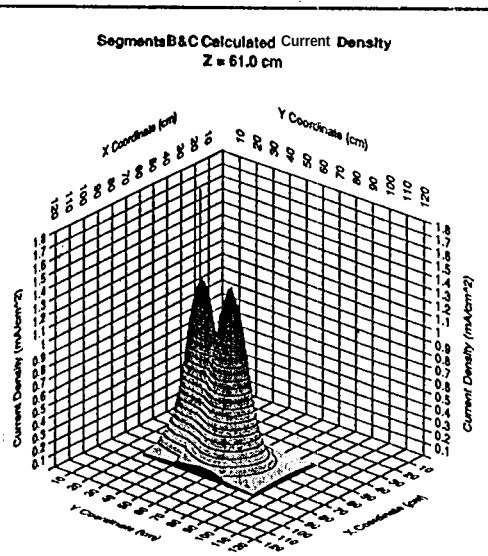

Figure 26

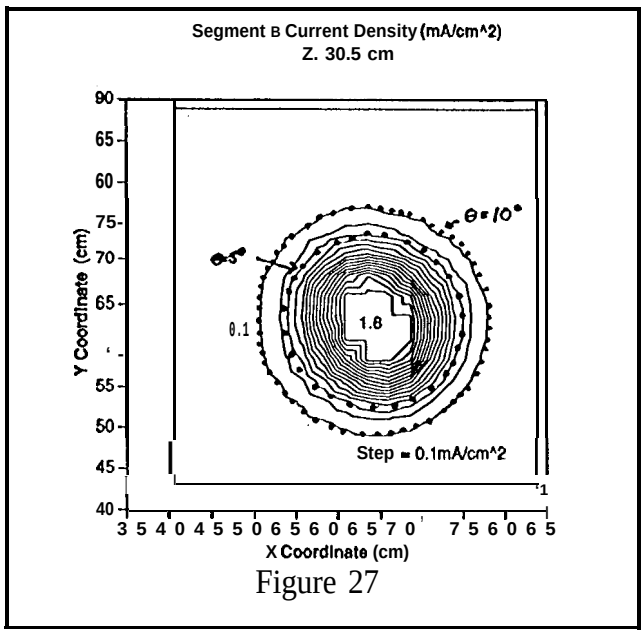

Figure 27

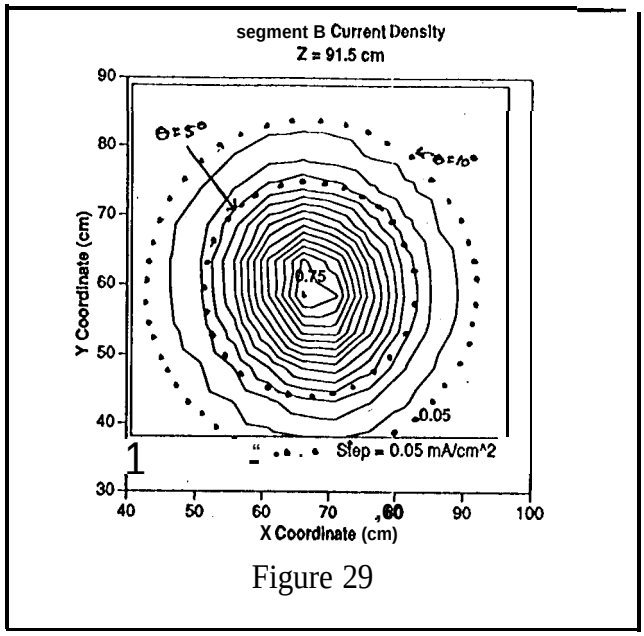

Figure 29

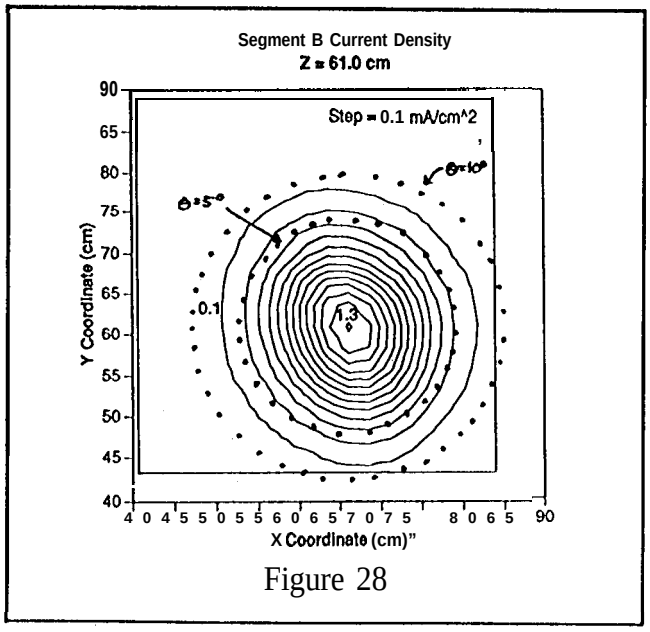

Figure 28

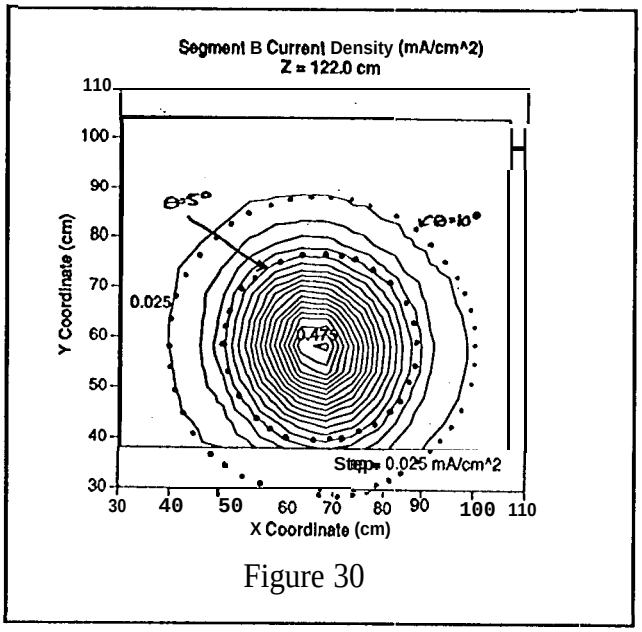

Figure 30

Ion Beam Divergence

As shown in Figs. 27-30, the circles corresponding to beam divergence angles of 5° and 10° are superimposed upon the 2-D current density contour plots for segment B. This was done for the four different Z positions relative to the thruster. According to these figures a relatively small portion of the beam exists outside of the 10° circle. More of the beam exists outside the 5° circle but still a relatively small amount. The ratio of ion beam concentration within the circle to that of the ion beam outside the circle seemed to remain constant as Z increased.

Conclusion

A numerical integration scheme was applied to the acquired data to determine the total beam current. These calculated values were generally within 5% of the values measured by the SIT power processing electronics. Asymmetries of the ion beam about the centerline were observed for segments A and C. The causes for these asymmetries arc as of yet unknown. A qualitative analysis of the downstream development of the ion beam was conducted, The widening of the beam and increase in uniformity of the current density were noticed. The reconstruction of current density profiles produced from simultaneous operation of multiple ion sources using data obtained from the operation of single ion sources was attempted. This exercise was limited in success. The calculated model did not display as high a current density level between the ion sources as did the measured. An initial look at the divergence of the plume suggests that the divergence angle is less than 100. Valuable trends pertaining to the development of ion plumes from the segmented ion thruster have been noted. However, most of the data acquired thus far has been on somewhat of a trial basis and was used to help get the bugs out of the system. This includes both operational difficulties with the segmented ion thruster and the data acquisition system used to collect the data, More extensive tests regarding the current density profiles of the segmented ion thruster arc scheduled to begin within 1 month.

Acknowledgments

The authors would like to thank Mr. Alison Owens, Mr. William Thogmartin, Mr. Robert Toomaath and Mr. Keith Goodfellow for their assistance in the development and operation of the segmented ion engine and support hardware.

The work described in this paper was performed by the Jet Propulsion Laboratory, California Institute of Technology, under contract with the National Aeronautics and Space Administration.

References

1 Mueller, J., Brophy, J.R., Brown, D. K., and Garner, C.E., "Segmented Ion Engine Operation and Performance,; AIAA-94-2851, presented at the 30th Joint Propulsion Conference, June 27-29, 1994, Indianapolis, IN.

2 Brophy, J.R., Pless, L. C., Mueller, J., and Anderson, J. R., "Operating Characteristics of a 15-cm-dia. ion Engine for Small Planetary Spacecraft," IEPC-93-110, presented at the 23rd International Electric Propulsion Conference, Scp 13-16, 1993, Seattle WA,

3 Patterson, M.J., Haag, T, W., and Hovan, S.A., "Performance of the NASA 30 cm Ion Thruster," IEPC-93-108, presented at the 23rd International Electric Propulsion Conference, Sep. 13-16, 1993, Seattle, WA, ,

4 Mueller, J., Brophy, J.R., and Garner, C.E., "Performance Characteristics of 15-cm Carbon-Carbon Composite Grids," AIAA-94-3118, to be presented at the 30th Joint Propulsion Conference, June 27-29, 1994, Indianapolis, IN.